CHALMERS
UNIVERSITY OF TECHNOLOGY

Terahertz radar observes powder dynamics for pharmaceutical manufacturing

Downloaded from: https://research.chalmers.se, 2024-06-30 15:03 UTC

Citation for the original published paper (version of record):
Bonmann, M., Moradikouchi, A., Bryllert, T. et al (2024). Terahertz radar observes powder dynamics for pharmaceutical manufacturing. IEEE Sensors Journal, 24(13): 20512-20522.
http://dx.doi.org/10.1109/JSEN.2024.3397399

N.B. When citing this work, cite the original published paper.

© 2024 IEEE. Personal use of this material is permitted. Permission from IEEE must be obtained for all other uses, in any current or future media, including reprinting/republishing this material for advertising or promotional purposes, or reuse of any copyrighted component of this work in other works.

This document was downloaded from http://research.chalmers.se, where it is available in accordance with the IEEE PSPB Operations Manual, amended 19 Nov. 2010, Sec, 8.1.9. (http://www.ieee.org/documents/opsmanual.pdf).

(article starts on next page)

This article has been accepted for publication in IEEE Sensors Journal. This is the author's version which has not been fully edited and content may change prior to final publication. Citation information: DOI 10.1109/JSEN.2024.3397399

Terahertz radar observes powder dynamics for pharmaceutical manufacturing

Marlene Bonmann, Anis Moradikouchi, Tomas Bryllert, Anders Sparen, Staffan Folestad, Jonas Johansson, Jan Stake, *Senior Member, IEEE*, and Helena Rodilla, *Senior Member, IEEE*

***Abstract*— The optical opaqueness of powders has precluded the observation of powder flow dynamics in processing tubes, with important implications, for example, in the pharmaceutical industry, where non-destructive monitoring during the manufacturing process is essential to ensure the quality of the final product and the effectiveness of the process. Taking advantage of the high penetration of terahertz electromagnetic waves in powders and its wavelength-to-particle size ratio, we demonstrate that a submillimeter-wave pulse-Doppler radar can overcome the present challenges and characterize powder flow dynamics in pharmaceutical manufacturing processes. Mimicking typical vessel shapes in pharmaceutical operations, we were able to characterize falling powder streams in a tube with a sample volume resolution of a few cubic centimeters and a range resolution of about 5 mm. We successfully monitored particle velocity, particle distribution within the tube, and mass flow rate in real-time. This remote sensing method, based on advanced terahertz electronics, opens up the possibility to study and monitor powder dynamics in a wide range of applications.**

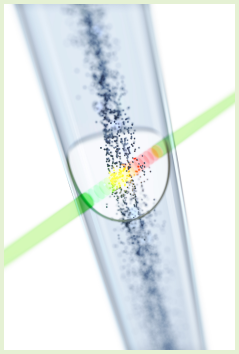

***Index Terms*— Doppler radar, Frequency-modulated continuous-wave (FMCW), Pharmaceuticals, Powders, Radars, Remote sensing, Submillimeter waves, THz sensors, Terahertz systems.**

I. Introduction

PHARMACEUTICAL manufacturing has, in recent years, started to transform from a traditional batch-based approach with fixed end-product quality parameters, to a science-based approach where quality is guaranteed by real-time process control and quality assurance using in-process monitoring and management [1]. In the pharmaceutical industry, solid oral dosage forms constitute almost 80% of the total drug products [2] and are produced by a sophisticated production chain that manipulates pharmaceutical ingredients in powder form. This manufacturing process faces typical powder-associated challenges like unpredictable powder flow dynamics, particle aggregation, bulk powder density variations, and powder content variations during processing. The flow properties of powders in the manufacturing process may affect the quality attributes of the final product, such as content uniformity, microstructure, weight, disintegration, and dissolution [3]. In batch manufacturing processes, quality assurance relies on several off-line tests on the final drug products, but as the pharmaceutical industry moves from batch towards continuous processing [4], [5], the integration of real-time process analytical tools into the manufacturing line that allows advanced in-process monitoring in manufacturing vessels becomes an essential requirement for quality assurance [6]. Even though effective process analytical tools have been developed to monitor the chemical quality attributes of powders, in-process analysis of physical phenomena, such as powder flow dynamics, powder density variations, and powder homogeneity, remains a challenge [7].

Typical non-destructive process analytical tools used in the pharmaceutical industry involve the short and mid-wavelength range of the electromagnetic spectrum, from X-rays to near-infrared regions. For instance, near-infrared spectroscopy is a common analytical technique introduced in the production line to assess the content of water and drug substances, as obtained from overtones and combinations of absorption bands corresponding to fundamental molecular vibrations [8], [9]. Raman spectroscopy is another common technique to quantify the drug substance [10] and blend homogeneity [11]. However, these techniques, which often require careful development and validation of robust multivariate calibration models and suffer from scattering effects, have a limited penetration depth of a few millimeters. The same occurs in the optical

This work was partly supported by the Swedish Foundation for Strategic Research (SSF) under the contracts ITM17-0265 and ID17-0011, and in part by AstraZeneca, Gothenburg, Sweden.

Marlene Bonmann was with the Terahertz and Millimetre Wave Laboratory, Chalmers University of Technology, SE-412 96 Gothenburg, Sweden. She is now with Infineon Technologies Austria AG, Villach, Austria.

Anis Moradikouchi was with Chalmers University of Technology and AstraZeneca, Gothenburg, Sweden. She is now with the Electrical and Computer Engineering Department at the University of California, Los Angeles, USA.

Staffan Folestad was with AstraZeneca, Gothenburg, Sweden. He is now with the Department of Industrial and Material Science, Chalmers University of Technology, SE-412 96 Gothenburg, Sweden.

Anders Sparen and Jonas Johansson are with AstraZeneca, Gothenburg, Sweden.

Tomas Bryllert, Jan Stake, and Helena Rodilla are with the Terahertz and Millimetre Wave Laboratory, Chalmers University of Technology, SE-412 96 Gothenburg, Sweden. (e-mail: rodilla@chalmers.se)

© 2024 IEEE. Personal use is permitted, but republication/redistribution requires IEEE permission. See https://www.ieee.org/publications/rights/index.html for more information.

This article has been accepted for publication in IEEE Sensors Journal. This is the author's version which has not been fully edited and
content may change prior to final publication. Citation information: DOI 10.1109/JSEN.2024.3397399

domain, which does not make it suitable for observing the flow dynamics of dense powder streams. On the other hand, using shorter wavelengths with high energy photons and high penetration, like in the case of X-ray tomography, comes with the price of long measurement and data processing times, which excludes this technique for in-line manufacturing applications [12]. Other methods like electrical capacitance measurements using low-frequency radio signals allow measurements of the concentration and flow of solid materials [13]. However, many capacitive probes are required to meet the need for high spatial resolution in large-scale process units. The terahertz frequency range [14], between the microwave and optical domain, has recently gained increasing attention for pharmaceutical applications [15]. Terahertz waves are less vulnerable to scattering effects than the infrared region, which provides more extended penetration depth and, therefore, can sense a larger sample volume [16]. Moreover, terahertz waves provide a smaller propagating beam and increased spatial resolution than microwave techniques since the diffraction-limit scales with the wavelength (λ). Terahertz spectroscopy has demonstrated promising results to characterize the physical properties of tablets like density and porosity [17]. An alternative to electromagnetic wave based methods is acoustic emission and active sonic techniques (echolocation), which can characterize the flow of solid powders [18]. Ultrasound imaging - at a wavelength similar to electromagnetic waves in the microwave and sub-terahertz region is a reliable, accurate, and non-invasive flow measurement technique [19]. However, contactless in-line monitoring of powder properties requires ultrasound transducers with an efficient acoustic coupling to the powder stream [7].

In this work, we propose a radar operating at terahertz frequencies to overcome the challenges preventing the real-time characterization of powder flow dynamics in the pharmaceutical production line of oral solid dosage forms. Radio detection and ranging (radar) is a standard microwave instrument for measuring the electromagnetic scattering of objects passing through the projected beam [20]. Depending on the radar modality, the received signal can be processed to estimate the distance, scattering properties, and the object's velocity through the Doppler effect [21]. Thanks to advancements in the terahertz technology, it is now possible to realize frequency-modulated continuous wave (FMCW) Doppler radar at submillimeter wavelengths [22], thereby providing high accuracy in position and velocity measurements in real-time, together with the ability to penetrate and sense through a powder stream. Moreover, the particle size and wavelength ratio of the terahertz wave results in a strong interaction through Mie scattering [23]. Terahertz radar systems have demonstrated the ability to characterize flow dynamics in fluidized bed reactors [24] and cloud dynamics [25]. Here, mimicking the typical vessel geometry in manufacturing operations, we demonstrated the ability of a terahertz pulse-Doppler radar [26] to characterize, in real-time, powder flow dynamics of powder particles falling through a tube. Particle flow velocity, concentration variations and particle distribution within the tube were recorded, demonstrating the terahertz radar as a promising remote diagnostic method for process control in pharmaceutical manufacturing with high industrial implementation capabilities.

II. Method

To investigate the ability of the terahertz radar to characterize the flow dynamics of pharmaceutical powders in processing pipes, we measured the reflected signal of falling microcrystalline cellulose (MCC) powder, a commonly used excipient in the pharmaceutical industry, inside a polymethyl methacrylate (PMMA) tube with a 340-GHz frequency-modulated continuous wave pulse-Doppler radar, see Fig. 1. Despite the typical stainless steel tubes used in pharmaceutical manufacturing processes, we used a transparent tube to enable visual inspection during the experiments. At the lower end of the tube, the powders landed on a container placed on top of a weighing scale that continuously recorded the accumulative powder weight that, together with the lapsed time, provided the mechanical mass flow rate. The mass flow rate was controlled by the number and size of the holes in the feed hopper. The almost collimated radar beam illuminated the particles that passed through the beam path. As a result of the scattering of the radar signal with the flowing particles, the radar receives a signal containing information on the particles' back-reflected scattering, also referred to as particle radar cross-section, σ, the velocity of the particles in the radar direction, and the optical distance of the particles relative to the instrument, referred as the range. The model used to obtain the physical properties of

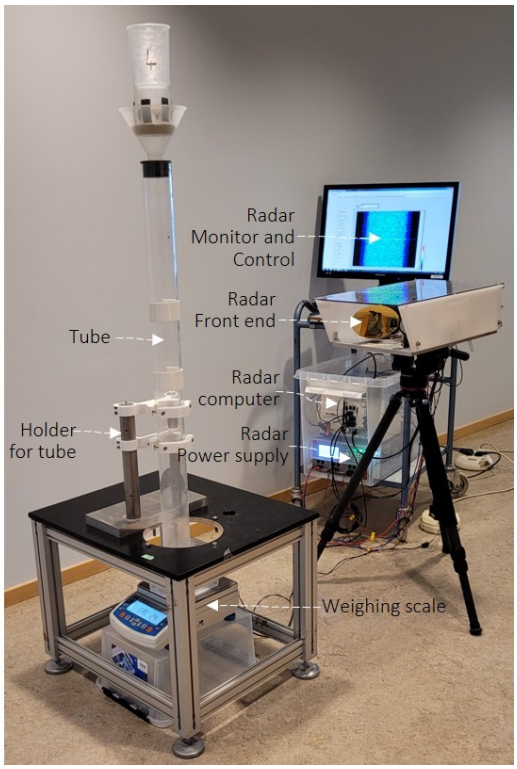

Fig. 1. Photograph of the experimental set-up. Chalmers terahertz particle radar illuminating the PMMA tube laterally. The weighing scale and the back-end electronics used for the pharmaceutical powder study can be observed in the photograph.

© 2024 IEEE. Personal use is permitted, but republication/redistribution requires IEEE permission. See https://www.ieee.org/publications/rights/index.html for more information.

This article has been accepted for publication in IEEE Sensors Journal. This is the author's version which has not been fully edited and content may change prior to final publication. Citation information: DOI 10.1109/JSEN.2024.3397399

the flowing particles from the radar signal model is described in Appendix I.

A. Terahertz particle radar

The radar instrument is a monostatic 340-GHz FMCW pulse-Doppler radar developed at Chalmers [26]. Linearly frequency-modulated pulses with a 30-GHz bandwidth of about milli-Watt output power are transmitted to the powder stream. The corresponding wavelength range (λ) of the radar signal is between 0.84 and 0.92 mm. The received signal of 128 pulses, within a coherent time of 6.6 ms, is computed to obtain the velocity profile and the position of the powder stream relative to the radiating horn antenna. A radar image frame interval of 346 ms was used. The instantaneous FMCW-bandwidth, $BW = 30$ GHz, provides a radar range resolution of approximately $\Delta R = c/(2 \times BW) = 5\,\text{mm}$. The optical system of the radar provides an almost collimated beam with a diameter of about 15 mm. The measured angular spread of the beam was 0.55 degrees. Hence, the sample volume resolution for the current set-up was about 1-2 cm^3. The back-reflected radar signal is proportional to the sample volume fraction, c_v, and the radar cross-section of the particle, σ. The powder velocity component along the radar beam is determined by the measured Doppler shift, f_D.

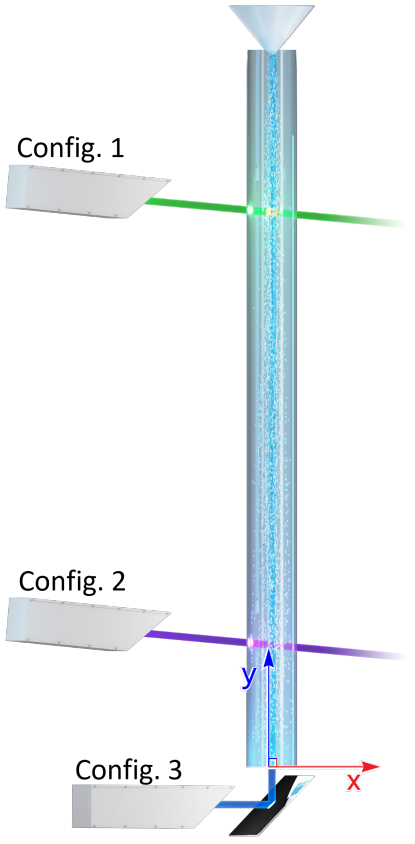

Fig. 2. Illustration of the three radar configurations used in this work. (Config. 1-2) Radar beam incident with an angle of $\boldsymbol{\theta = 5°}$ from the side at a distance of about 154 cm from the tube. Config. 1 with the radar at the upper part of the tube, $\boldsymbol{y = 84}$ cm and Config. 2 with the radar at the lower part of the tube, $\boldsymbol{y = 23}$ cm. (Config. 3) By using a mirror, the radar beam was redirected and incident from the bottom of the tube, vertically, along the stream. The total beam path from the radar to the tube was 107 cm.

B. Set-up

The set-up was designed to establish a controlled powder stream inside the tube to mimic the powder flow in a continuous pharmaceutical production line. First, the powders were dispensed in plastic feed hoppers with a conical bottom with evenly distributed orifices. The size and number of orifices are used to control the powder mass flow rate. The feed hopper was located on a cylindrical tube with air gaps to allow air intake from the surroundings, minimizing the pulsing effects of the powder stream. The powder strings from the hopper holes enter a funnel and form a single powder stream at the exit of the lower opening of the funnel, which we call the outlet. The size of the outlet determines the cross-section of the powder stream. The powder particles flow vertically through the PMMA tube, which has a height of 100 cm, an outer diameter of 7 cm, and a 3-mm wall thickness. The mass, m, of the particles landing on the container on top of the weighing scale was recorded every 328 milliseconds. The time derivative of the cumulative powder weight gives the mass flow rate, $\dot{m}$, calculated using the forward difference method.

Fig. 2 shows the three different configurations used to study the powder stream dynamics. One of them has the radar beam incident from the bottom of the tube parallel to the stream (config. 3 in Fig. 2), and the other two have the radar beam incident from the side of the tube, one of them with the radar located at the upper part of the tube ($y = 84$ cm) and the other with the radar at the lower part of the tube ($y = 23$ cm), see config. 1 and config. 2 in Fig. 2. For the two cases with the beam incident from the side of the tube, a slight angle θ of the incident beam is needed to detect a Doppler shift of the downfall velocity component, v_y, and to redirect strong reflections from the tube walls. In this work, we used an incident angle $\theta \sim 5\,\text{deg}$ with the horizontal coordinate. The measured distance, x_θ, and velocity, v_θ, can be written as a function of the radar beam inclination angle θ and reference coordinates like:

$$v_\theta = v_x \cos\theta + v_y \sin\theta \tag{1a}$$

$$x_\theta = (x - x_0)\cos\theta + (y - y_0)\sin\theta. \tag{1b}$$

For the configuration with the beam incident from the bottom of the tube parallel to the stream, a flat mirror located under the tube was used to redirect the beam inside the tube. The total beam path between the radar and the lower tube opening was about 107 cm. For the measurement with the beam incident from the side, the radar was located about 154 cm from the tube.

C. Mechanical mass flow rate measurements

The mechanical mass flow rate was computed as $\dot{m} = \Delta m/\Delta t$, where m was the weight measured with a RADWAG PS 10100.R2.M Precision Balance, and Δt was the time

© 2024 IEEE. Personal use is permitted, but republication/redistribution requires IEEE permission. See https://www.ieee.org/publications/rights/index.html for more information.

This article has been accepted for publication in IEEE Sensors Journal. This is the author's version which has not been fully edited and
content may change prior to final publication. Citation information: DOI 10.1109/JSEN.2024.3397399

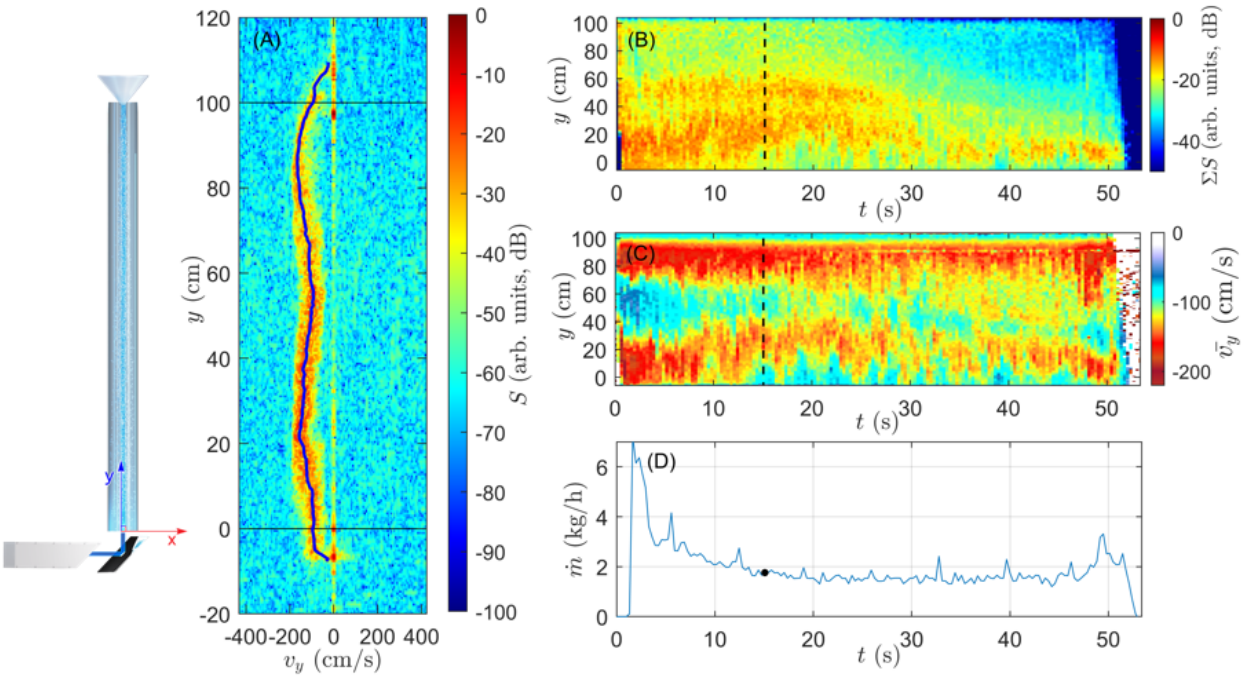

Fig. 3. Powder flow of MCC-100 along the tube. On the left is an illustration of the radar configuration used to obtain the results presented in this figure. (A) Radar image showing the intensity of the reflected radar signal, $\boldsymbol{S}$, as a function of the velocity of the particles towards the radar, $\boldsymbol{v_y}$, and position along the tube length, $\boldsymbol{y}$. The continuous blue line represents the instantaneous mean velocity obtained from the velocity distribution for each range bin, and the solid horizontal black lines indicate the tube edges. Time evolution of (B) the total radar signal, $\sum_{\boldsymbol{v_y}} \boldsymbol{S}$, and (C) instantaneous average velocity, $\bar{\boldsymbol{v}}_{\boldsymbol{y}}$, along tube length, $\boldsymbol{y}$. The moment when the radar image presented in 1A was taken is marked with a discontinuous black line. (D) The mechanical mass flow rate was recorded during the experiment with the weighing scale. The time corresponding to the results presented in 1A was highlighted with a black dot.

between consecutive balance read-outs, which was set to 0.328 s, the same as the time between radar image frames. The balance measures every 0.1 s, but only the value sent before the 0.328 s readout time is recorded. This measurement procedure is responsible for the peaks appearing in the mechanical mass flow rate measurements approximately every 7 seconds when the measuring and recording times align to a multiple of a second. The stabilization time of the balance was 1.5 s.

III. Results

A. Radar characterization of flow dynamics

The radar images of falling MCC obtained with the radar beam incident from the bottom of the tube, parallel to the stream, are shown in Fig. 3. The median diameter of the MCC particles was about 100 μm (MCC-100). Fig. 3A shows one radar image corresponding to an exposure of the powder stream to 128 coherent pulses during a time interval of 6.6 ms. The measured velocity of the powder particles in the radar direction, v_y, and the intensity of the back-reflected radar signal, S, can be observed along the tube length, y. Notice that the particle velocity measured by the radar is the component onto the radar's line of sight. The continuous blue line in the figure represents the instantaneous mean velocity, $\bar{v}_y$, obtained from the velocity probability distribution of powder particles for each range bin. As shown in Fig. 3A, the velocity distribution was narrow, indicating that all particles moved with similar velocity. They were accelerating from the hopper outlet, decelerating at the middle of the tube, and accelerating again. Fig. 3B shows the time evolution of $\sum_{v_y} S$, which is the sum of the radar signal across the velocity axis at each position bin. S is proportional to the volume concentration of the powder particles, c_v. However, in our measurement setup, the radar beam crosses the powder particles accumulated over time in the container beneath the tube, resulting in the signal attenuation over time observed in Fig. 3B. The time evolution of the instantaneous mean velocity $\bar{v_y}$ is shown in Fig. 3C. Consistently with Fig. 3A, the mean velocity is always higher at the top and bottom than in the center of the tube.

How the powder flow evolves inside a tube is a complex phenomenon - a consequence of the interaction between the powder particles and the gas phases inside the tube - and depends on particles' properties and concentration [27]. Fig. 4 shows the ability of the terahertz radar to characterize different flow dynamics inside a tube. A comparison of vertical radar images of MCC with two different particle sizes and two different mass flow rates is presented. To illustrate the complex interaction, a free fall model for a single particle (see Appendix II) of respective size has been included in the plots for comparison. In Fig. 4A can be observed that, for the case with a lower mass flow rate and particle diameter of 100 μm, the free-fall model doesn't adjust to the experimental results, and instead, as already observed in Fig. 3A, a particles deceleration was observed when the particles pass by the middle of the tube. For the same particles falling under a higher mass flow rate (Fig. 4B), the particles deceleration in the middle of the tube was still apparent, but the velocity probability distribution

© 2024 IEEE. Personal use is permitted, but republication/redistribution requires IEEE permission. See https://www.ieee.org/publications/rights/index.html for more information.

This article has been accepted for publication in IEEE Sensors Journal. This is the author's version which has not been fully edited and content may change prior to final publication. Citation information: DOI 10.1109/JSEN.2024.3397399

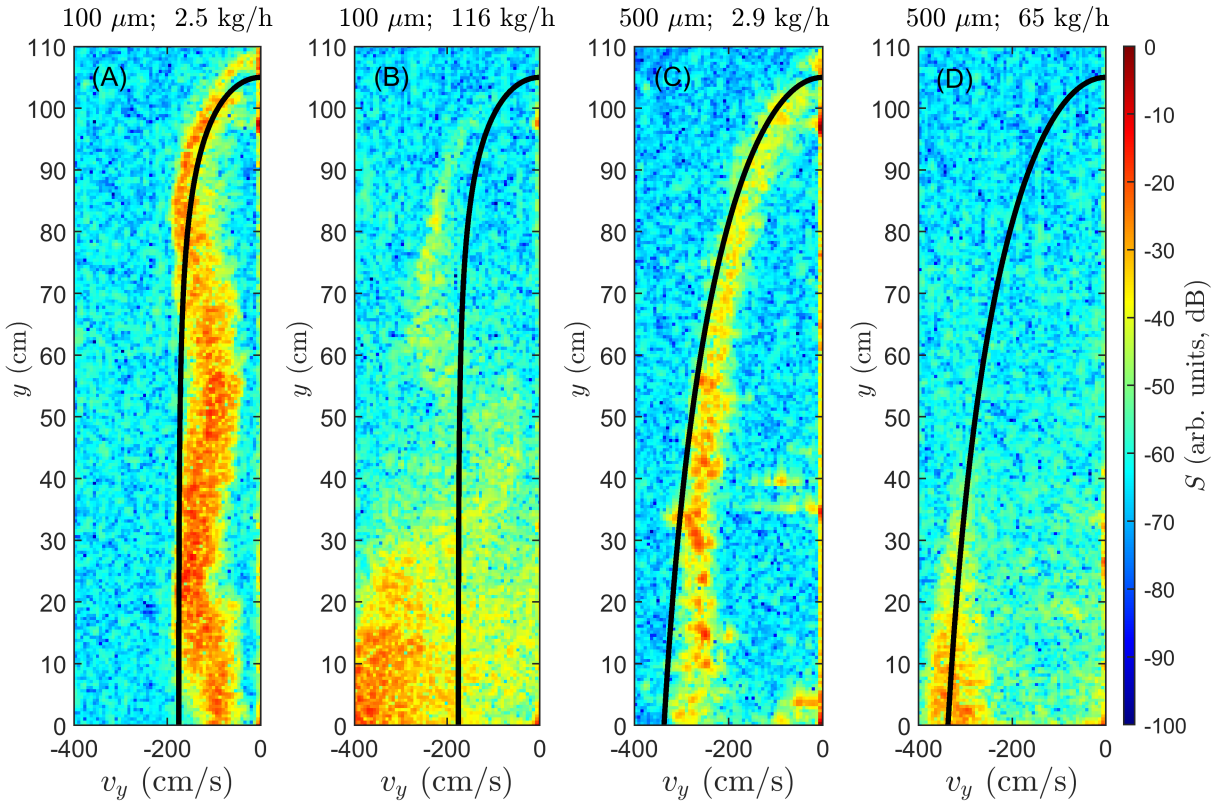

Fig. 4. Radar observation of different flow dynamics. Radar images showing different types of flow inside the tube for two different particle sizes and two different mass flow rates. The intensity of the reflected radar signal, S, is plotted as a function of the velocity of the particles towards the radar, v_y, and tube length, y, with the radar beam incident from the bottom of the tube, being the beam parallel to the flow. (A) MCC with a median particle diameter of 100 μm (MCC-100) and a low mass flow rate, (B) MCC-100 with a high mass flow rate, (C) MCC with a median particle diameter of 500 μm (MCC-500) and a low mass flow rate, and (D) MCC-500 with a high mass flow rate. The continuous black line represents the analytical solution for the free fall of a single particle moving vertically under gravity and quadratic air resistance derived from solving Newton's second law of motion (see method section). The mechanically measured mass flow rates for MCC-100 were around 2.5 kg/h and 116 kg/h for the low and high flow, respectively. For MCC-500, around 2.9 kg/h and 65 kg/h (the accompanying mechanical mass flow rate graphs can be seen in Fig. S4)

becomes wider, and the velocity at the end of the tube is larger. The observed increased terminal velocity compared to the one obtained with the single-particle free-fall model has been previously reported and can be explained by a smaller effective air drag acting on the particles when the particle concentration is high [28]. On the other hand, the larger the particle diameter, the closer the velocity of the particles in the stream agrees with the single particle model [27]. Indeed, Figs. 4C-D show that the velocity trajectory for the bigger particles is close to the one obtained using the free fall model for a single particle. Notice that Fig. 4B and 4D suffer from a high attenuation of the radar signal consequence of the high particle concentration stored on the particle´s container under the tube for the higher mass flow rate.

B. Lateral characterization

The set-up configuration with the radar beam along the stream used in Figs. 3-4 demonstrates the strength of the radar to non-intrusively monitor different powder flow dynamics along the tube length. However, this configuration is challenging to implement in a real production line. Fig. 5 shows the radar images obtained for falling MCC-100 with a mass flow rate similar to the results in Fig. 3, but with the radar beam incident from the side of the tube, which can be easily implemented into the pharmaceutical processing line. To study the evolution of the flow dynamics at different tube heights, the radar was located at two positions: at the upper part of the tube, Figs. 5(A-D), and at the lower part of the tube, Figs. 5(E-H). In the radar image presented in Fig. 5A, the radar signal shows that at the top of the tube, the powder stream presents a centered main core. The measured velocity of the powder particles towards the radar, v_θ, has a contribution from the two velocity vector components, v_y and v_x. In this context, the increased velocity observed close to the second wall of the tube is a signature of a diverging behavior of the powder stream from the center to the side of the tube, In other words, the centered powder stream is expanding. Real-time monitoring of $\sum_{v_y} S$ and $\bar{v_\theta}$ (Figs. 5B and 5C, respectively) show the time variability of the velocity and signal, i.e., the flickering of the powder stream. When the radar was located on the lower part of the tube, a more evenly distributed mean velocity and radar signal across the tube walls was observed (Fig. 5F), with the maximum mean velocity in the center of the tube (Fig. 5G), indicating that the powder particles have mainly a vertical velocity component, v_y, with little diverging behavior. These results were consistent with the visual inspection through the

© 2024 IEEE. Personal use is permitted, but republication/redistribution requires IEEE permission. See https://www.ieee.org/publications/rights/index.html for more information.

This article has been accepted for publication in IEEE Sensors Journal. This is the author's version which has not been fully edited and
content may change prior to final publication. Citation information: DOI 10.1109/JSEN.2024.3397399

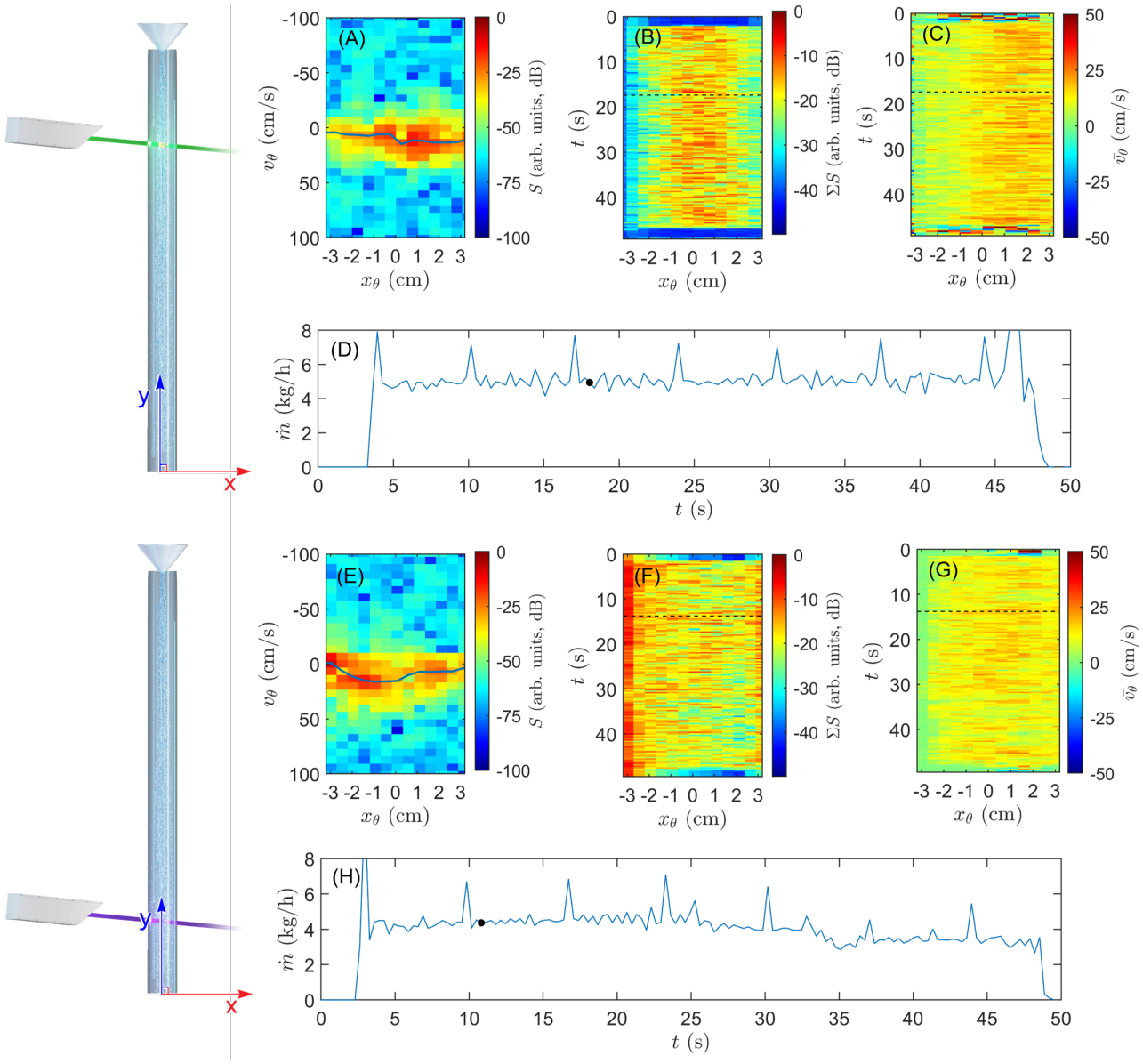

Fig. 5. Lateral characterization of the powder flow of MCC-100. (A) Radar image showing the intensity of the reflected radar signal, $\boldsymbol{S}$, as a function of the particles velocity towards the radar, $\boldsymbol{v_\theta}$, and the cross-section of the tube projected in the radar direction, $\boldsymbol{x_\theta}$, when the radar beam was incident from the side, on the upper part of the tube (configuration shown schematically at the top left figure). The continuous blue line represents the instantaneous mean velocity obtained from the velocity distribution for each range bin $\boldsymbol{\bar{v}_\theta}$. (B) and (C) show the time evolution of the total radar signal, $\sum_{v_\theta} \boldsymbol{S}$, and $\bar{v}_\theta$ along the projected cross-section of the tube, $\boldsymbol{x_\theta}$. A discontinuous black line was used to mark in the time-dependent plots the time when the single radar image presented in Fig. A was taken. (D) The mass flow rate recorded during the flowing process for the upper configuration, where the time when Fig. A was recorded is marked with a black dot. The peaks shown every 7 seconds arise as an artifact of the precision balance readout configuration (see methods section for further information). (E - H), correspond to Figs. A-D when the radar beam was incident from the side at the lower part of the tube (configuration shown schematically at the bottom left of the figure). All measurements were taken for flowing MCC-100.

transparent tube, where a dense and narrow flow stream of about a fourth of the tube width was observed at the top of the tube. The stream was observed to diverge, and the core separated into several denser powder strings along the tube, filling the powder stream the whole tube diameter at the lower part of the tube. Furthermore, the core and the powder strings flickering in position observed by the radar were also visually observed.

The velocity and density profiles of the particles across the tube for two different mass flow rates are presented and compared to non-existing flow in Fig. 6. Here, we chose two extreme cases of flow rate: a low mass flow rate of $\sim$ 4.5 kg/h and a high mass flow rate of $\sim$ 120 kg/h. All for the falling MCC-100 powder particles. The average radar signal, $< \sum_{v_\theta} S >$, and the average mean velocity, $< \bar{v_\theta} >$, were calculated over the ten consecutive radar images. The mechanical mass flow rate measured during the averaging time is highlighted in red in Figs. 6F, which corresponds to 3.5 seconds. It must be noted that static energy inside the tube walls creates variable, unpredictable results in the vicinity of

© 2024 IEEE. Personal use is permitted, but republication/redistribution requires IEEE permission. See https://www.ieee.org/publications/rights/index.html for more information.

This article has been accepted for publication in IEEE Sensors Journal. This is the author's version which has not been fully edited and
content may change prior to final publication. Citation information: DOI 10.1109/JSEN.2024.3397399

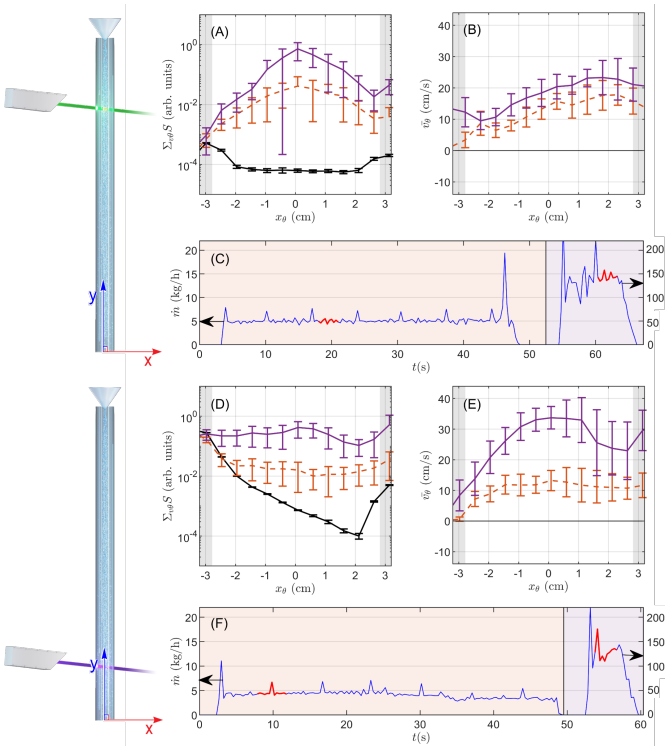

Fig. 6. Remote sensing of density and velocity profiles at different mass flow rates. (A) Averaged radar signal, $< \sum_{\boldsymbol{v_\theta}} \boldsymbol{S} >$, and (B) averaged mean velocity, $< \bar{\boldsymbol{v}}_{\boldsymbol{\theta}} >$, along the projected tube cross-section, $\boldsymbol{x_\theta}$, both with the radar located on the side of the tube at the top position (illustration on the top left). (C) Mechanical mass flow rate recorded over time during the experiments where Fig. A-B where obtained. First for the mass flow rate of around 4.5 kg/h, followed by the one of around 120 kg/h. The time corresponding to the frames used for calculating the average signal and velocity are highlighted in red. (D - F) correspond to Figs. A-C when the radar beam was incident from the side at the lower part of the tube (configuration shown schematically at the bottom left of the figure). The regions marked in grey are affected by static energy, so results must be variable and inconsistent in these regions.

the tube walls, an area marked in grey in the plots. The higher particle density associated with the higher mass flow rate was detected by the radar by a stronger radar signal, see Figs. 6A and D. In terms of particle distribution across the tube, as in Fig. 5, a non-uniform powder distribution within the tube walls was observed at the top of the tube, with a high volume concentration of particles at the center (Fig. 6 A), and a more uniform particle distribution was seen at the bottom position, Fig. 6C. Figs. 6B and 6D also showed that the powder streams with higher mass flow rates had higher average mean velocity, which also agrees with the observation of the vertical measurements for the low and high mass flow rates shown in Fig. 4A-B.

C. Mass flow rate monitoring from lateral measurements

The ability of terahertz radar measurements to provide vertical velocity with an incoming radar beam from the side of the tube is demonstrated in Fig. 7. Here, MCC-100 particles were flowing, and measurements were recorded with the radar located at the side of the tube at the lower position with different incident angles. This radar position was selected for its previously observed non-diverging powder stream, and as a consequence, almost negligible horizontal velocity component, v_x. Fig. 7A shows the expected negligible velocity towards the radar for an incident angle of $0\,\mathrm{deg}$, and how the velocity increases as the incident angle increases. In Fig. 7B, the angle-dependent measurements obtained from the side of the tube were compared with a vertical measurement projected to the respective angle, demonstrating good agreement.

Fig. 7C shows an example of the capability of the radar side measurements to monitor real-time mass flow rate. These results are for flowing MCC-100 particles with two different mass flow rates and using an incident angle $\theta = 5\,\mathrm{deg}$. The falling mass flow is directly proportional to the velocity, obtained from v_θ, and to the volume concentration of the particles, which was obtained from the radar signal. The flow stream diameter was assumed to be the same as the inner diameter of the tube, which is a reasonable assumption for this radar position. A good agreement between the mechanical and radar mass flow rates was demonstrated. The mass flow rate fluctuations captured by the radar can not be attributed to noise; see the noise level in Fig 7C between 50 s and 58 s where there is no flow. The weighing scale did not capture these fluctuations due to the averaging and time readout of the scale. Moreover, it must be noted that the assumption of a constant flow along the tube´s cross-section has some limitations, which could also be partially responsible for the oscillations. A moving average filter over 4 seconds allows smoothing of the radar mass flow rate to a level comparable to the mechanical one. From these results, we can conclude that radar side measurements are valid for real-time monitoring of mass flow rate, a parameter of interest in pharmaceutical operations. This is of particular interest when the vertical realization of the radar system is troublesome, as in most industrial applications.

IV. Conclusion

We demonstrated the ability of a terahertz radar system to non-invasively characterize, in real-time, the flow dynamics of pharmaceutical powders in a tube, with promising implementation capabilities in the manufacturing processes. Powder particles flowed through a vertical tube to mimic typical vessel shapes in pharmaceutical operations. Side and vertical radar measurements were carried out to measure the particles velocity, density distribution, and their variation versus distance and time. In this work, we could easily see through an MCC powder flow with a stream diameter of 7 cm and a mass flow rate of 120 kg/h. The powder flow density/volume concentration and velocity profiles were obtained from the radar signal. In addition, we showed that real-time mass flow rate could be obtained from side measurements via the radar signal and velocity. This could be of great interest in industrial applications where powder flow distribution, density, and mass flow rate are critical parameters, and vertical realization of sensing systems can be impractical. Thanks to progress in terahertz radar engineering, this part of the electromagnetic spectrum can be utilized for process analysis for monitoring and characterizing flowing powders for pharmaceutical applications and many other industrial manufacturing processes where powder and particle flow characterization is critical.

© 2024 IEEE. Personal use is permitted, but republication/redistribution requires IEEE permission. See https://www.ieee.org/publications/rights/index.html for more information.

This article has been accepted for publication in IEEE Sensors Journal. This is the author's version which has not been fully edited and
content may change prior to final publication. Citation information: DOI 10.1109/JSEN.2024.3397399

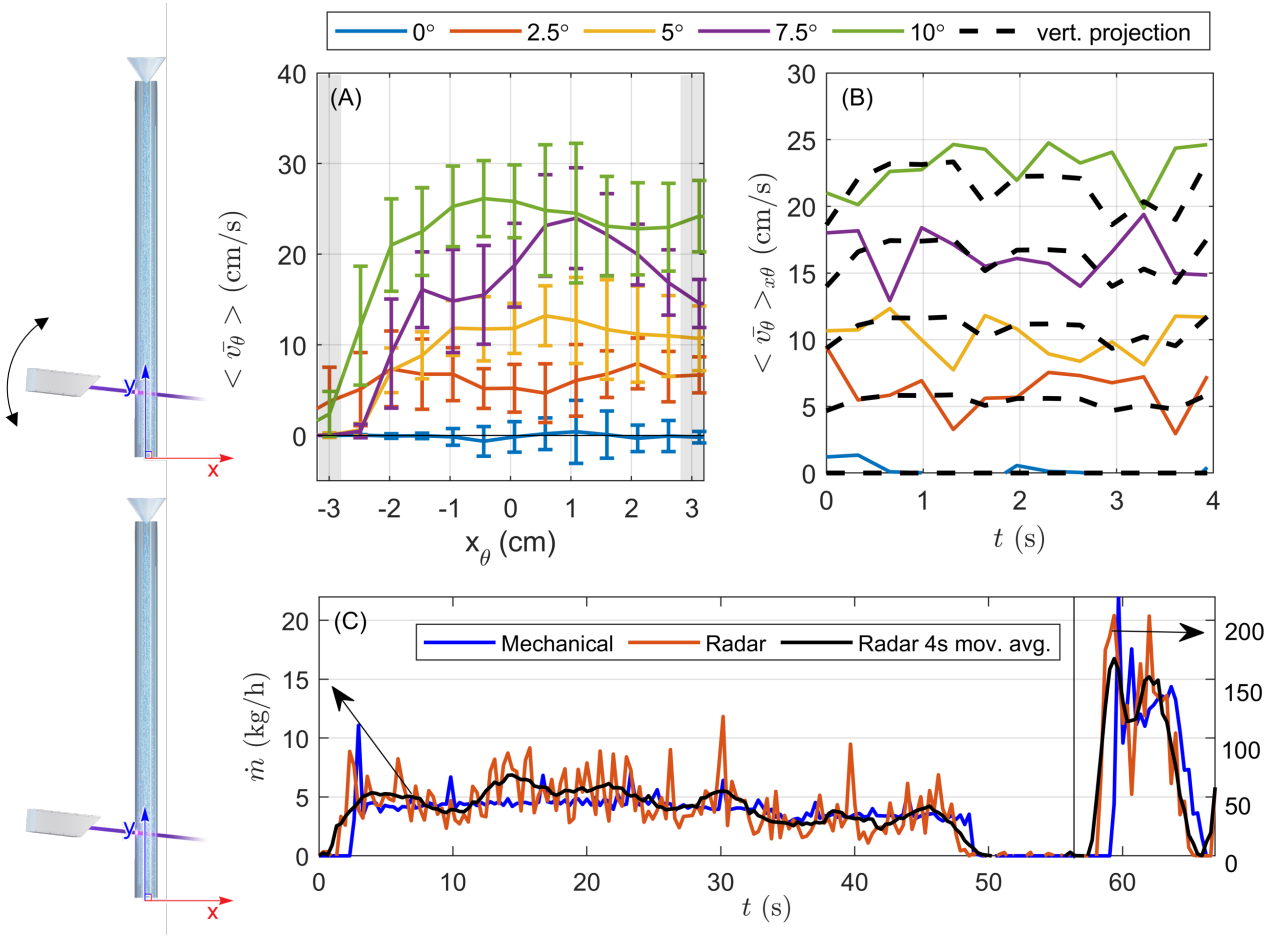

Fig. 7. Remote sensing of mass flow rate from lateral measurements. Results for MCC-100 with the radar located in the lower side of the tube. (A) Averaged mean velocity, $< \bar{v}_{\boldsymbol{\theta}} >$, along the projected tube cross-section, $\boldsymbol{x_\theta}$, for different incident angles, $\boldsymbol{\theta}$. The regions marked in gray are affected by static energy, so results must be variable and inconsistent in these regions. (B) Cross section mean velocity of $< \bar{v}_{\boldsymbol{\theta}} >_{\boldsymbol{x\theta}}$ versus time for different $\boldsymbol{\theta}$ (continuous line) compared to projected vertical measurements (dashed lines). The results presented in A and B had mass flow rates between 3-6 kg/h and were averaged over ten consecutive radar images. (C) Radar mass flow rate obtained through the measured radar signal and velocity compared with the mechanical mass flow rate obtained with the weighing scale. A moving average filter over 4 seconds for the radar measurements was also included. The radar location is shown on the bottom left of the figure and had $\boldsymbol{\theta = 5\,\mathrm{deg}}$.

APPENDIX I
PARTICLE CLOUD RADAR SIGNAL MODEL

This appendix summarizes the mathematical models used to analyze pharmaceutical powders' dynamics and physical properties using pulse-Doppler radar measurements. The methodology was initially proposed by Bonmann *et al.* for glass, sand, and bronze particles with a diameter similar to the wavelength [29].

The received power, P_r, from a single scattering target can be derived from Friis's transmission formula [30], which results in the famous radar equation:

$$P_r = \frac{P_t A_e^2 L}{4\pi\lambda^2}\frac{\sigma}{R^4}, \tag{2}$$

where P_t is the transmitted power, A_e is the effective antenna area, L is the loss factor, λ is the radar wavelength, σ is the radar cross-section, also called radar signature, and R is the range, i.e., the distance between target and radar. Hence, the received radar signal S, which includes the transfer function of the radar hardware and free space path loss, is proportional to the radar cross-section and inversely proportional to the range, R^4, (optical distance) as:

$$S \propto \frac{\sigma}{R^4}. \tag{3}$$

When the size of the scattering particles is comparable to the wavelength, the scattering is not necessarily isotropic. The portion of the scattered signal reflected backwards is calculated using Mie theory [23]. The backscattering cross-section for a single spherical particle is then given by:

$$\sigma_b = \pi r^2 Q_b, \tag{4}$$

where r is the particle radius and Q_b is the backscattering efficiency calculated with the help of the Mie formalism implemented in MATLAB functions written by [31]. The scattering efficiencies depend on the particle's refractive index and size, and the wavenumber of the surrounding medium. In this work, values of σ_b of 2.65×10^{-10} m^2 and 6.86×10^{-8} m^2 for MCC-100 and MCC-500 respectively were calculated.

The radar will sense a sampling volume, V_{sample}, of particles illuminated by the beam with a radius, w, and within

© 2024 IEEE. Personal use is permitted, but republication/redistribution requires IEEE permission. See https://www.ieee.org/publications/rights/index.html for more information.

This article has been accepted for publication in IEEE Sensors Journal. This is the author's version which has not been fully edited and content may change prior to final publication. Citation information: DOI 10.1109/JSEN.2024.3397399

the radar range resolution, ΔR. Thus, for a low number of particles per volume, the total cross-section area for the radar sampling volume $V_{sample} = \pi w^2 \Delta R$ can be defined as:

$$\sigma_{tot} = V_{sample} c_n \sigma, \tag{5}$$

where c_n is the number of particles per volume. The influence of multi-scattering between particles is neglected, which is a valid assumption for wavelength-sized particles and volume fractions below 2.4×10^{-4} according to work by Mishchenko et al. [32]. The volume fraction c_v of the particle cloud is then:

$$c_v = V_{particle} c_n = \frac{4}{3}\pi r^3 c_n, \tag{6}$$

where $V_{particle}$ is the volume of a single particle. Combining the above equations, the radar signal can now be formulated as:

$$S \propto \frac{\sigma_b}{R^4} c_v \frac{V_{sample}}{V_{particle}}. \tag{7}$$

For a cloud of particles of a homogeneous material, the radar signal is directly proportional to the volume fraction, c_v.

The shift in frequency, or the Doppler frequency $f_D = 2v_\theta/\lambda$, provides the velocity distribution v of the particles within the sampling volume. The mean velocity of the distribution is denoted as $\bar{v}$.

The mass flow rate is given by the closure of the mass balance

$$\dot{m} = \frac{dm}{dt} = c_v \rho A |v_y| \tag{8}$$

where ρ is the density of the particles, A is the cross-sectional area of the particle stream, and v_y is the velocity of the particles along the tube. Thus, the mass flow rate can be estimated from radar measurements and compared with mass measurements with a weighing scale versus time. Combining equations 7-8, the mass flow is proportional to radar signal S and its Doppler shift (velocity) as:

$$\dot{m} \propto S |v_y| \tag{9}$$

APPENDIX II
SINGLE PARTICLE FREE FALL MODEL

The time evolution of the velocity, v, and position, y, of a particle under vertical free fall, considering air resistance, was modeled as:

$$v = v_t tanh(t/\tau) \tag{10}$$

$$y = y_0 - v_t \tau ln(cosh(t/\tau)) \tag{11}$$

with the terminal velocity $v_t = \sqrt{2mg/(A\rho_{air}c_d)}$ and the characteristic time $\tau = v_t/g$, where g is the gravitational constant, m the mass of the particle, calculated from the particle density of MCC and the respective particle size, ρ_{air} the air density (1.29 kg/m^3 room temperature pressure), A the particle cross-section, c_d the drag coefficient, t is the time under free-fall, and y_0 is the initial position. The value of c_d depends on the Reynolds number, R_e, which is calculated as $R_e = (\rho_{air} u D)/\mu$, where u is the mean velocity of the surrounding medium (air), D is the diameter of the pipe, and μ the dynamic viscosity of the surrounding. Assuming the air velocity is similar to the measured particle velocity, the Reynolds number lies in the interval $10^3 - 10^4$, and the drag coefficient for a fixed sphere becomes $c_d = 0.4$ [33], which was used for calculations.

ACKNOWLEDGMENT

The authors thank Mats Myremark for machining mechanical parts for the measurement setup, and Dr. David Pallares, Dr. Carolina Guio Perez and Dr. Johan Remmelgas for the fruitful discussions and feedback. The team conducted the experiments in the Kollberg Laboratory at the Chalmers University of Technology, Gothenburg, Sweden.

REFERENCES

[1] J. Rantanen and J. Khinast, "The future of pharmaceutical manufacturing sciences," *Journal of Pharmaceutical Sciences*, vol. 104, no. 11, pp. 3612–3638, 2015. doi: 10.1002/jps.24594.

[2] E. Emery, J. Oliver, T. Pugsley, J. Sharma, and J. Zhou, "Flowability of moist pharmaceutical powders," *Powder Technology*, vol. 189, no. 3, pp. 409–415, 2009. doi: 10.1016/j.powtec.2008.06.017.

[3] D. Markl and J. A. Zeitler, "A Review of Disintegration Mechanisms and Measurement Techniques," *Pharmaceutical Research*, vol. 34, no. 5, pp. 890–917, 2017. doi: 10.1007/s11095-017-2129-z.

[4] K. Plumb, "Continuous processing in the pharmaceutical industry: Changing the mind set," *Chemical Engineering Research and Design*, vol. 83, no. 6 A, 2005. doi: 10.1205/cherd.04359.

[5] M. Ierapetritou, F. Muzzio, and G. Reklaitis, "Perspectives on the continuous manufacturing of powder-based pharmaceutical processes," *AIChE Journal*, vol. 62, no. 6, 2016. doi: 10.1002/aic.15210.

[6] S. Laske, A. Paudel, O. Scheibelhofer, S. Sacher, T. Hoermann, J. Khinast, A. Kelly, J. Rantannen, O. Korhonen, F. Stauffer, F. De Leersnyder, T. De Beer, J. Mantanus, P. F. Chavez, B. Thoorens, P. Ghiotti, M. Schubert, P. Tajarobi, G. Haeffler, S. Lakio, M. Fransson, A. Sparen, S. Abrahmsen-Alami, S. Folestad, A. Funke, I. Backx, B. Kavsek, F. Kjell, M. Michaelis, T. Page, J. Palmer, A. Schaepman, S. Sekulic, S. Hammond, B. Braun, and B. Colegrove, "A Review of PAT Strategies in Secondary Solid Oral Dosage Manufacturing of Small Molecules," 2017. doi: 10.1016/j.xphs.2016.11.011.

[7] S. Stranzinger, D. Markl, J. G. Khinast, and A. Paudel, "Review of sensing technologies for measuring powder density variations during pharmaceutical solid dosage form manufacturing," *TrAC - Trends in Analytical Chemistry*, vol. 135, p. 116147, 2021. doi: 10.1016/j.trac.2020.116147.

[8] P. Frake, D. Greenhalgh, S. Grierson, J. Hempenstall, and D. Rudd, "Process control and end-point determination of a fluid bed granulation by application of near infra-red spectroscopy," *International Journal of Pharmaceutics*, vol. 151, no. 1, pp. 75–80, 1997. doi: 10.1016/S0378-5173(97)04894-1.

[9] O. Berntsson, L. G. Danielsson, B. Lagerholm, and S. Folestad, "Quantitative in-line monitoring of powder blending by near infrared reflection spectroscopy," *Powder Technology*, vol. 123, no. 2-3, 2002. doi: 10.1016/S0032-5910(01)00456-9.

[10] I. Jedvert, M. Josefson, and F. Langkilde, "Quantification of an active substance in a tablet by NIR and Raman spectroscopy," *Journal of Near Infrared Spectroscopy*, vol. 6, no. 1-4, 1998. doi: 10.1255/jnirs.148.

[11] G. J. Vergote, T. R. De Beer, C. Vervaet, J. P. Remon, W. R. Baeyens, N. Diericx, and F. Verpoort, "In-line monitoring of a pharmaceutical blending process using FT-Raman spectroscopy," *European Journal of Pharmaceutical Sciences*, vol. 21, no. 4, 2004. doi: 10.1016/j.ejps.2003.11.005.

[12] L. Farber, G. Tardos, and J. N. Michaels, "Use of X-ray tomography to study the porosity and morphology of granules," *Powder Technology*, vol. 132, no. 1, pp. 57–63, 2003. doi: 10.1016/S0032-5910(03)00043-3.

[13] M. G. Rasteiro, R. C. C. Silva, F. A. P. Garcia, and P. M. Faia, "Electrical tomography: a review of configurations and applications to particulate processes," *KONA Powder and Particle Journal*, vol. 29, p. 67–80, 2011. doi: 10.14356/kona.2011010.

[14] M. Tonouchi, "Cutting-edge terahertz technology," *Nature Photonics*, vol. 1, no. 2, pp. 97–105, 2007. doi: 10.1038/nphoton.2007.3.

[15] P. Bawuah and J. A. Zeitler, "Advances in terahertz time-domain spectroscopy of pharmaceutical solids: A review," 6 2021. doi: 10.1016/j.trac.2021.116272.

© 2024 IEEE. Personal use is permitted, but republication/redistribution requires IEEE permission. See https://www.ieee.org/publications/rights/index.html for more information.

This article has been accepted for publication in IEEE Sensors Journal. This is the author's version which has not been fully edited and
content may change prior to final publication. Citation information: DOI 10.1109/JSEN.2024.3397399

[16] P. H. Siegel, "Terahertz technology," *IEEE Transactions on Microwave Theory and Techniques*, vol. 50, no. 3, pp. 910–928, 2002. doi: 10.1109/22.989974.
[17] D. Markl, P. Bawuah, C. Ridgway, S. van den Ban, D. J. Goodwin, J. Ketolainen, P. Gane, K.-E. Peiponen, and J. A. Zeitler, "Fast and non-destructive pore structure analysis using terahertz time-domain spectroscopy," *International Journal of Pharmaceutics*, vol. 537, no. 1, pp. 102–110, 2018. doi: 10.1016/j.ijpharm.2017.12.029.
[18] C. Davies, S. Tallon, and N. Brown, "Continuous monitoring of bulk density and particle size in flowable powders and grains," *Chemical Engineering Research and Design*, vol. 83, p. 782–787, July 2005. doi: 10.1205/cherd.04325.
[19] C. Poelma, "Ultrasound imaging velocimetry: a review," *Experiments in Fluids*, vol. 58, 2016. doi: 10.1007/s00348-016-2283-9.
[20] "Radio detection and ranging," *Nature*, vol. 152, p. 391–392, 1943. doi: 10.1038/152391b0.
[21] C. A. Doppler, "Über das farbige Licht der Doppelsterne und einiger anderer Gestirne des Himmels," *Abh. Königl. Böhm. Ges. Wiss.*, vol. 2, pp. 465–482, 1843.
[22] K. B. Cooper and G. Chattopadhyay, "Submillimeter-wave radar: Solid-state system design and applications," *IEEE Microwave Magazine*, vol. 15, pp. 51–67, Nov. 2014. doi: 10.1109/mmm.2014.2356092.
[23] G. Mie, "Beiträge zur optik trüber medien, speziell kolloidaler metallösungen," *Annalen der Physik*, vol. 330, no. 3, pp. 377–445, 1908. doi: 10.1002/andp.19083300302.
[24] D. C. Guío-Pérez, M. Bonmann, T. Bryllert, M. Seemann, J. Stake, F. Johnsson, and D. Pallarès, "Radar-based measurements of the solids flow in a circulating fluidized bed," *Fuel*, vol. 345, p. 128232, 2023. doi: 10.1016/j.fuel.2023.128232.
[25] K. B. Cooper, R. Rodriguez Monje, R. J. Dengler, C. J. Cochrane, M. Alonso-Delpino, A. Tang, T. O. El Bouayadi, and O. Pradhan, "A compact, low power consumption, and highly sensitive 95 GHz Doppler radar," *IEEE Sensors Journal*, vol. 20, no. 11, pp. 5865–5875, 2020. doi: 10.1109/JSEN.2020.2972535.
[26] T. Bryllert, M. Bonmann, and J. Stake, "A submillimeter-wave FMCW pulse-Doppler radar to characterize the dynamics of particle clouds," *IEEE Transactions on Terahertz Science and Technology*, vol. 13, no. 4, pp. 389–395, 2023. doi: 10.1109/TTHZ.2023.3263641.
[27] T. Uchiyama, "Numerical analysis of particulate jet generated by free falling particles," *Powder Technology*, vol. 145, no. 2, pp. 123–130, 2004. doi: 10.1016/j.powtec.2004.06.004.
[28] K. Ogata, K. Funatsu, and Y. Tomita, "Experimental investigation of a free falling powder jet and the air entrainment," *Powder Technology*, vol. 115, no. 1, pp. 90–95, 2001. doi: 10.1016/S0032-5910(00)00329-6.
[29] M. Bonmann, D. Carolina Guío-Pérez, T. Bryllert, D. Pallarès, M. Seemann, F. Johnsson, and J. Stake, "Sub-millimetre wave range-Doppler radar as a diagnostic tool for gas-solids systems - solids concentration measurements," *Advanced Powder Technology*, vol. 34, no. 1, p. 103894, 2023. doi: 10.1016/j.apt.2022.103894.
[30] H. Friis, "A note on a simple transmission formula," *Proceedings of the IRE*, vol. 34, no. 5, pp. 254–256, 1946. doi: 10.1109/JRPROC.1946.234568.
[31] C. Mätzler, "Matlab functions for mie scattering and absorption, version 2," tech. rep., Institute of Applied Physics, University of Bern, 2002. doi: 10.7892/boris.146550.
[32] M. I. Mishchenko, L. Liu, and G. Videen, "Conditions of applicability of the single-scattering approximation," *Opt. Express*, vol. 15, pp. 7522–7527, Jun 2007. doi: 10.1364/OE.15.007522.
[33] D. G. Miller and A. B. Bailey, "Sphere drag at Mach numbers from 0·3 to 2·0 at Reynolds numbers approaching 10^7," *Journal of Fluid Mechanics*, vol. 93, pp. 449–464, Aug. 1979. doi: 10.1017/s0022112079002597.

Marlene Bonmann was born in Karlsruhe, Germany, in 1988. She received an M.Sc. degree in physics and astronomy and a Ph.D. in Microtechnology and Nanoscience from the Chalmers University of Technology, Gothenburg, Sweden, in 2014 and 2020, respectively.

From 2020 to 2023, she was a Postdoctoral Researcher with the Terahertz and Millimetre Wave Laboratory. At the end of 2023, she joined Infineon Technologies AG, where she is currently working with the manufacture of semiconductor devices.

Anis Moradikouchi was born in Fasa, Iran, in 1990. She received an M.Sc. degree in Electrical Engineering from Shiraz University, Iran, and a Ph.D. in Microtechnology and Nanoscience from the Chalmers University of Technology, Gothenburg, Sweden, in 2016 and 2023, respectively.

Anis Moradikouchi is currently a postdoctoral scholar at UCLA Terahertz Electronics Laboratory.

Tomas Bryllert was born in Växjö, Sweden, in 1974. He received an M.Sc. degree in physics and a Ph.D. in semiconductor physics from Lund University, Lund, Sweden, in 2000 and 2005, respectively.

In 2006, he joined the Microwave Electronics Laboratory at Chalmers University of Technology, Göteborg, Sweden. From 2007 to 2009, he was with the Submillimeter Wave Advanced Technology (SWAT) group, Jet Propulsion Laboratory, California Institute of Technology, Pasadena, CA, USA. He is currently with the Terahertz and Millimetre Wave Laboratory at Chalmers University of Technology, Göteborg, Sweden. He is also the co-founder and Chief Executive Officer of Wasa Millimeter Wave AB, a company that develops and fabricates millimeter wave products. Dr. Bryllert also works part-time in the new concepts team at Saab AB. His research interests include submillimeter wave electronic circuits and their applications in imaging and radar systems.

Anders Sparén was born in Luleå, Sweden, in 1958. He received an MSc in chemical engineering and a PhD in analytical chemistry from the Royal Institute of Technology in Stockholm, Sweden, in 1988 and 1994, respectively.

Anders joined Astra in 1995 and today he holds a position as an associate principal scientist in chemical/formulation characterization with vibrational spectroscopy at AstraZeneca Gothenburg, Sweden. His current focus is on process analytical technology, machine learning, and data management applied to continuous manufacturing.

© 2024 IEEE. Personal use is permitted, but republication/redistribution requires IEEE permission. See https://www.ieee.org/publications/rights/index.html for more information.

This article has been accepted for publication in IEEE Sensors Journal. This is the author's version which has not been fully edited and content may change prior to final publication. Citation information: DOI 10.1109/JSEN.2024.3397399

Staffan Folestad was born in Örebro, Sweden, in 1954. He received his PhD in Chemistry from the University of Göteborg in 1985.

In 1994, he joined Astra Hässle and worked as a senior principal scientist. He was head of AstraZeneca CoE for Process Analytical Technology, working on implementing advanced in-situ Process Sensors, in silico Process Modeling, and Quality by Design (QbD) approaches. He held global responsibility for Pharmaceutical Innovation in the Materials and Manufacturing Sciences area, leading the associated Strategy Development and External Liaison between 2015 and 2022. In addition, he conducted part-time academic research as an Adjunct Professor at Uppsala University between 1999 and 2005 and thereafter affiliated with Chalmers University of Technology. Staffan Folestad is currently a guest scholar at Chalmers University of Technology after retiring in 2022 as Director of Science and Innovation from AstraZeneca. He has 28 years of experience in industrial Pharmaceutical Product and Process Development. His most recent research addresses challenges in systems engineering design, specifically patient-centric pharmaceutical product and production design and unified solutions for mass customization, personalization, and individualization.

Dr. Folestad is an elected member of the Royal Swedish Academy of Engineering Sciences (IVA) and received the “New Safe Medicines Faster Award 2007” from the European Federation of Pharmaceutical Sciences.

Jonas Johansson was born in Lund, Sweden in 1960. He received a M.Sc. in Engineering Physics and a Ph.D. in Atomic Physics in 1987 and 1993, respectively.

From 1993 to 1997, he was a Research Associate at Lund Institute of Technology, Sweden, and received a position as a Senior Master in 1997. He was appointed Associate Professor in 2001 and Adjunct Professor in 2007 at Lund Institute of Technology, Sweden. From 1997 to 2024, he was an employee at AstraZeneca Gothenburg, Sweden. He has held roles as a Scientist, Associate Principal Scientist, Principal Scientist, Team Manager, Associate Director, Science & Technology Lead, Science & Innovation Director, and Senior Director of Science & Innovation. His main research interest is vibrational spectroscopy applied to the pharmaceutical industry.

Dr. Johansson serves as an expert for the European Innovation Council.

Jan Stake (S’95–M’00–SM’06) was born in Uddevalla, Sweden, in 1971. He received an M.Sc. in electrical engineering and a Ph.D. in microwave electronics from Chalmers University of Technology in Gothenburg, Sweden, in 1994 and 1999, respectively.

In 1997, he was a Research Assistant at the University of Virginia, Charlottesville, VA, USA. From 1999 to 2001, he was a Research Fellow with the Millimetre Wave Group at the Rutherford Appleton Laboratory, Didcot, UK. He then joined Saab Combitech Systems AB, Gothenburg, Sweden, as a Senior RF/microwave Engineer until 2003. From 2000 to 2006, he held different academic positions with the Chalmers University of Technology, and from 2003 to 2006, he was also the Head of the Nanofabrication Laboratory, Department of Microtechnology and Nanoscience (MC2). In 2006, he was appointed Professor and the Head of the Terahertz and Millimetre Wave Laboratory at the Chalmers University of Technology. He was a Visiting Professor with the Submillimeter Wave Advanced Technology (SWAT) Group at Caltech/JPL, Pasadena, CA, USA, in 2007 and at TU Delft, the Netherlands, in 2020. He is also the co-founder of Wasa Millimeter Wave AB, Gothenburg, Sweden. His research interests include high-frequency semiconductor devices, terahertz electronics, submillimeter wave measurement techniques, and terahertz systems.

Prof. Stake served as the Editor-in-Chief for the IEEE Transactions on Terahertz Science and Technology between 2016 and 2018 and as Topical Editor between 2012 and 2015. From 2019 to 2021, he was chairman of the IEEE THz Science and Technology Best Paper Award committee. He is an elected member of the International Society of Infrared, Millimeter and Terahertz Waves (IRMMW-THz) board.

Helena Rodilla (M’16–SM’20) was born in Salamanca, Spain, in 1982. She received the B.S. and Ph.D. degrees in Physics from the University of Salamanca, Salamanca, Spain, in 2006 and 2010, respectively.

From 2006 to 2010, she was with the Electronics Group, Department of Applied Physics, University of Salamanca, Spain, where her research interest was semiconductor physics. From 2011 to 2013, she was a Postdoctoral Researcher with the Microwave Electronics Laboratory, Department of Microtechnology and Nanoscience (MC2), Chalmers University of Technology, Gothenburg, Sweden, where she worked on InP HEMTs for cryogenic low-noise amplifiers. Since 2013 she has been with the Terahertz and Millimetre Wave Laboratory, MC2, Chalmers University of Technology, Gothenburg, Sweden, where she became an Associate Professor in 2020. Her current research interests include millimeter wave and terahertz technology in life science applications, sensing, and on-wafer terahertz measurements.

Dr. Rodilla serves as Associate Editor for the IEEE Transactions on Terahertz Science and Technology since 2018.

© 2024 IEEE. Personal use is permitted, but republication/redistribution requires IEEE permission. See https://www.ieee.org/publications/rights/index.html for more information.